RKKY signals characterizing the topological phase transitions in Floquet Dirac semimetals

Hou-Jian Duan,* Shi-Ming Cai, Xing Wei, Yong-Chi Chen, Yong-Jia Wu, Ming-Xun Deng, Ruiqiang Wang,† and Mou Yang
Guangdong Basic Research Center of Excellence for Structure and Fundamental Interactions of Matter, Guangdong Provincial Key Laboratory of Quantum Engineering and Quantum Materials, School of Physics, South China Normal University, Guangzhou 510006, China and Guangdong-Hong Kong Joint Laboratory of Quantum Matter, Frontier Research Institute for Physics, South China Normal University, Guangzhou 510006, China

(Received 3 January 2024; revised 1 April 2024; accepted 8 May 2024; published 23 May 2024)

Recently, the Floquet Na_3Bi-type material has been proposed as an ideal platform for realizing various phases, i.e., the spin-degenerate Dirac semimetal (DSM) can be turned into the Weyl semimetal (WSM), and even to the Weyl half-metal (WHM). Instead of the conventional electrical methods, we use the RKKY interaction to characterize the topological phase transitions in this paper. It is found that detecting the Ising term J_I is feasible for distinguishing the phase transition of DSM/WSM, since the emergence of J_I is induced by the broken spin degeneracy. For the case with impurities deposited on z axis (the line connecting the Weyl points), the Heisenberg term J_H coexists with J_I in the WSM, while J_H is filtered out and only J_I survives in the WHM. This magnetic filtering effect is a reflection of the fully spin-polarized property (one spin band is in the WSM phase while the other is gapped) of the WHM, and it can act a signal to capture the phase transition of WSM/WHM. This signal can not be disturbed unless the direction of the impurities greatly deviates from z axis. Interestingly, as the impurities are moved into the x-y plane, there arises another signal (a dip structure for J_H at the phase boundary), which can also identify the phase transition of WSM/WHM. Furthermore, we have verified that all magnetic signals are robust to the term that breaks the electron-hole symmetry. Besides characterizing the phase transitions, our results also suggest that the Floquet DSMs are power platforms for controlling the magnetic interaction.

DOI: 10.1103/PhysRevB.109.205149

I. INTRODUCTION

The study of the topological states has become a hot topic in condensed matter and it recently excited a great interest in realizing various topological phases, including topological insulators and topological semimetals. One powerful method to generate topological states is to apply electromagnetic radiation, which can rearrange the band structure and change material properties by photon dressing [1–10]. For example, topological Weyl semimetals (WSMs) can be obtained by applying a beam of circularly polarized light (CPL) in nodal-line semimetals [7] or Dirac semimetals (DSMs) [8,9]. Usually, these so-called Floquet topological states can be controlled by the light intensity (or frequency), and the optical tunability offers the related materials a great potential for applications in spintronics. Remarkably, the Floquet topological states have been experimentally realized in artificial photonic lattices [11], as well as in the solid [12].

Recently, the Na_3Bi-type DSM has attracted us due to the various topological phases induced by the off-resonant CPL [13]. As stated in Ref. [13], the original DSM is changed to be a WSM once the light is turned on. More interestingly, besides the WSM, the Weyl half-metal (WHM) can be obtained if the light intensity exceeds a critical value. Compared to the WSM, the WHM possesses greater potential for the development of spintronic devices since it acts as a perfect spin filter in the Dirac-Weyl semimetal junction. This transport property is resulting from the fully spin-polarized property of the WHM, i.e., one spin band is in the WSM phase while the other is in the insulator phase. The discovery of the various phases in Floquet DSMs raises an interesting topic: how to detect these topological phases? To solve this problem, a conventional method is to measure the spin-resolved quantum Hall conductivity or probe the surface states directly. However, the accuracy of these methods is highly dependent on the purity of the materials, since impurities or defects are unavoidable in real materials. Moreover, the surface states are susceptible to the disturbance from bulk states in topological semimetals. Thus, new methods for probing the phase transitions are necessary.

The RKKY interaction between magnetic impurities offers the possibility for detecting the phase transitions, since it is sensitive to the deformation of the band structure of the materials. Typically, magnetic signals can be extracted from the amplitude, the oscillation, and the decaying laws of the RKKY interaction for characterizing the properties of the materials. For example, the amplitude of the RKKY interaction contributed by the edge states is about 20 times greater than the bulk contribution in the silicene nanoribbon [14], the tilting effect of the bands are characterized by the RKKY components in Dirac [15] and Weyl materials [16], the interfacial chiral bound states can be identified by the

*dhjphd@163.com
†wangruiqiang@m.scnu.edu.cn

nondecaying amplitude of the RKKY interaction in Dirac and Weyl systems [17], the significant difference in the amplitude of the RKKY interaction can act as a signal to distinguish between the topological Fermi surface and the trivial Fermi surface in nodal-line semimetal [18], the anisotropic decaying laws of the RKKY interaction can be used as the evidence that the semi-DSMs (S-DSMs) are distinct from other isotropic systems [19], the splitting of the Weyl points in WSMs can be captured by the oscillation of the RKKY interaction [20–22]. Besides the static systems, the RKKY interaction has also recently been explored in irradiated systems [23–25], where the RKKY interaction can be controlled via a Floquet drive due to the sensitivity of the interaction to the photon-dressed band.

Correlating the RKKY interaction with the topological phase transitions is a novel topic since there is very few literature in this area. As far as we know, the only successful example is Ref. [14], which has succeeded in identifying the phase transitions in silicene by using the edge-states-mediated RKKY interaction. Even so, almost no literature has succeeded in establishing a relationship between the bulk-states-mediated RKKY interaction and the topological phase transitions. In this paper, by doping magnetic impurities in the bulk of the Floquet Na_3Bi-type DSM, it is expected that signals can be extracted from the RKKY interaction to characterize the various phase transitions. Since we mainly focus on the long-range (i.e., relatively large impurity distance) configurations, one can assume that the external impurities do not affect the low-energy band structure, as discussed in Ref. [26]. By further considering the off-resonant condition of the CPL and following the treatment (i.e., the direct interaction between the impurities and the itinerant electrons is assumed to be constant even in the light field) employed in Refs. [24,25], the RKKY interaction can be calculated by the standard perturbation theory with the aid of the static (time-independent) Green's function. It is found that the RKKY components have completely different responses to the light parameters in different phases. By checking the Ising term, the phase transition of DSM/WSM can be identified. Depending on the impurity configuration, different signals in the Heisenberg term can be used to ascertain the phase boundary between the WSM and the WHM. Furthermore, the fully spin-polarized property of the WHM can also be reflected on the RKKY interaction. In addition, we have discussed the effect of the broken electron-hole symmetry on the magnetic signals. From these discussions, we have proved that the RKKY interaction can be used as an effective method for probing the phase transitions in Na_3Bi-type DSMs. Also, we have revealed that the Floquet DSMs are great platforms for controlling the magnetic interaction.

Our paper is organized as follows. In Sec. II, the low-energy model of the Floquet Na_3Bi-type DSM is introduced, and various phase transitions are exhibited. In addition, the method for calculating the RKKY interaction is raised. In Sec. III, the RKKY interaction in different phases are discussed with impurities placed in different directions. In Sec. IV, the term breaking the electron-hole symmetry is added and its effects on the magnetic signals are discussed. Finally, a summary is drawn in Sec. V.

II. MODEL AND METHOD

We start with a Floquet DSM model introduced in Refs. [27,28], where Na_3Bi and Cd_3As_2 act as the prototypes of the DSMs. The corresponding low-energy Hamiltonian in orbital and spin basis of $(|S,\frac{1}{2}\rangle, |P,\frac{3}{2}\rangle, |S,-\frac{1}{2}\rangle, |P,-\frac{3}{2}\rangle)$ can be written as

$$H(\mathbf{k}) = \begin{pmatrix} \epsilon_0(\mathbf{k}) + \mathbf{h}_+(\mathbf{k})\cdot\tau & \mathbf{0} \\ \mathbf{0} & \epsilon_0(\mathbf{k}) + \mathbf{h}_-(\mathbf{k})\cdot\tau \end{pmatrix} \quad (1)$$

with

$$\begin{aligned} \epsilon_0(\mathbf{k}) &= C_0' + C_1 k_z^2 + C_2 k_\parallel^2, \\ \mathbf{h}_s(\mathbf{k}) &= \left(s v_s k_x,\ -v_s k_y,\ M_0' - M_1 k_z^2 - M_2 k_\parallel^2 - s\lambda\right), \end{aligned} \quad (2)$$

where $k_\parallel^2 = k_x^2 + k_y^2$, $C_0' = C_0 + C_2 k_A^2$, $M_0' = M_0 - M_2 k_A^2$, $\lambda = v_0^2 k_A^2/(\hbar\Omega)$, and $v_s = v_0 - s v_A$ with $v_A = 2v_0 M_2 k_A^2/(\hbar\Omega)$. Here, k_A and Ω refer to the light intensity and frequency, respectively, $\tau = (\tau_x, \tau_y, \tau_z)$ is the vector of Pauli matrix in orbital space, and the subscript $s = +(-)$ for spin up (down). Noting that all terms in Eq. (2) related to k_A are induced by applying a beam of off-resonant light to the DSMs (a detailed derivation is given in Appendix A). The diagonal term $\epsilon_0(\mathbf{k})$ in $H(\mathbf{k})$ of Eq. (1) breaks the electron-hole symmetry and M_0' in $h_s(\mathbf{k})$ acts as the Dirac mass. By diagonalizing the Hamiltonian of Eq. (1), the energy dispersion can be solved as

$$E_{s,s'}(\mathbf{k}) = \epsilon_0(\mathbf{k}) + s'\sqrt{\left(M_0' - M_1 k_z^2 - M_2 k_\parallel^2 - s\lambda\right)^2 + v_s^2 k_\parallel^2}, \quad (3)$$

where $s' = +(-)$ refers to the conduction (valence) band. From Eqs. (2)–(3), one can see that there are two main effects induced by the light. One is that the parameters C_0 and M_0 are modified by the new terms $C_2 k_A^2$ and $-M_2 k_A^2$, respectively. The former would shift all the bands downward in the energy direction and the latter would change the positions of the Dirac points. Even so, the spin degeneracy of the system is still undisturbed. Another effect is that new spin-dependent terms $-s\lambda\tau_z - v_A(k_x\tau_x - s k_y\tau_y)$ are generated to break the time-reversal symmetry (TRS). In this scenario, the spin-up band $E_{+,s'}$ and the spin-down band $E_{-,s'}$ would exhibit different responses to k_A. Naturally, the spin degeneracy of the Dirac points can be destroyed.

Interestingly, along with the broken spin degeneracy come various topological phases for different k_A, as stated in Ref. [13]. To observe the phase transitions intuitively, we plot the energy dispersions of k_z axis in Fig. 2, where ϵ_0 is temporarily dropped (i.e., $\epsilon_0 = 0$). For $k_A = 0$, the bands are spin degenerated and the system stays in the DSM phase [Fig. 2(a)]. Due to $M_{0/1} < 0$, there exists two Dirac points with positions $(0, 0, \pm k_0)$ $(k_0 = \sqrt{M_0/M_1})$, each of which contains two spin-resolved Weyl points with opposite chiralities, as shown in Fig. 1. Different from the paired Weyl points at the same Dirac point in conventional DSMs, the overlapped Weyl points here are nonpaired and protected from mixing by the $\mathbb{Z}_2$ symmetry [13]. Considering the block-diagonal form of the Hamiltonian $H(\mathbf{k})$ [Eq. (1)] in spin space, one can find that only the Weyl points with opposite chiralities and the same spin can form a pair, i.e., Weyl partners are locked with

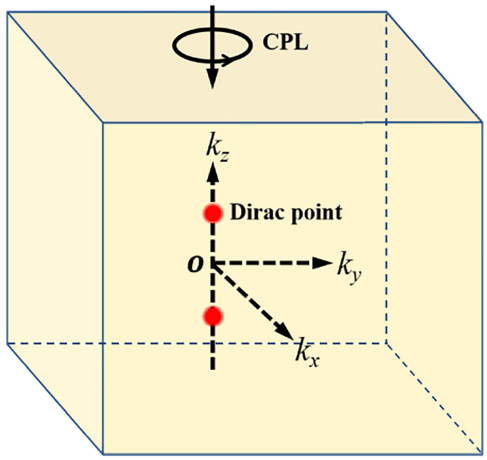

FIG. 1. Schematic of Na_3Bi-type DSMs with two Dirac points located on k_z axis with positions $(0, 0, \pm k_0)$ ($k_0 = \sqrt{M_0/M_1}$), each of which contains two spin-resolved Weyl points with opposite chiralities. Along z axis, a beam of off-resonant CPL is assumed to be irradiated.

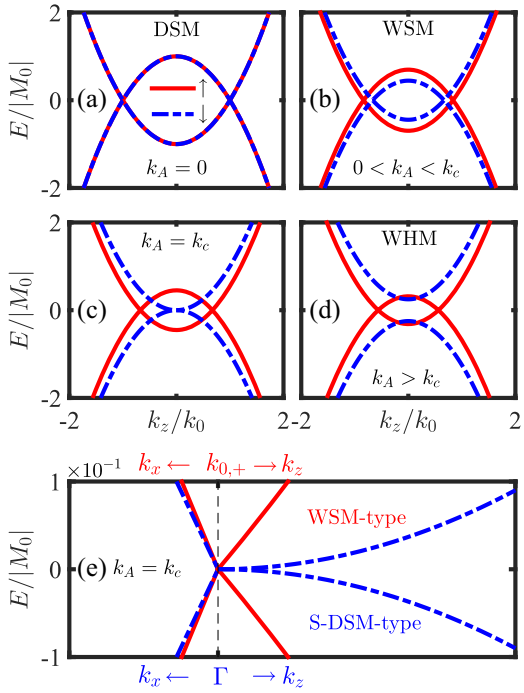

FIG. 2. Evolution of the k_z-axis dispersion with different values of k_A, which change the material from (a) DSM to (b) WSM, and then to (d) WHM. The solid (dashed) lines denote the spin-up (spin-down) bands. (c) The k_z-axis dispersion for the phase boundary ($k_A = k_c$) between the WSM and the WHM. The related low-energy dispersion is shown in (e), where the spin-up band around the Weyl point $k_{0,+}$ is linear in all directions while the spin-down band exhibits a semi-Dirac shape around the Γ point (i.e., linear in k_x axis but disperses quadratically in k_z axis). Here, $k_{0,+} = \sqrt{(M_0 - M_2 k_A^2 - \lambda)/M_1}$, $k_c = \sqrt{M_0/(M_2 - v_0^2/\hbar\Omega)}$ with $\hbar\Omega = 2$ eV and ϵ_0 is temporarily dropped (i.e., $\epsilon_0 = 0$). Parameters $M_0 = -0.08686$ eV, $M_1 = -10.6424$ eV Å^2, $M_2 = -10.3610$ eV Å^2, $v_0 = 2.4598$ eV Å are extracted from Na_3Bi [27] material.

spin. Once a small k_A is considered, i.e., $0 < k_A < k_c$ with $k_c = \sqrt{M_0/(M_2 - v_0^2/\hbar\Omega)}$, the two pairs of Weyl partners are separated due to the different responses of the spin-up and spin-down bands to k_A [Fig. 2(b)]. Consequently, the original DSM is transformed to be a WSM, whose Weyl points are located at $(0, 0, \pm k_{0,s})$ with $k_{0,s} = \sqrt{(M_0 - M_2 k_A^2 - s\lambda)/M_1}$. As $k_A > k_c$ is satisfied, the system enters into the WHM phase. Compared to the WSM, the key characteristic of the WHM is the fully spin-polarized property, i.e., one spin band is in the WSM phase while the other is in the insulator phase, as shown in Fig. 2(d). Due to the peculiar band structure, only the electrons of one spin band are allowed to participate in the transport when the Fermi energy u_F is inserted in the gap of the other spin band. Based on this property, the WHM has been proposed as a perfect spin filter [13]. If a large k_A with $k_A > \sqrt{M_0/(M_2 + v_0^2/\hbar\Omega)}$ is considered, the material is changed to be a normal insulator, where all bands are gapped. In this paper, we only focus on the topological phases (DSM, WSM, and WHM) since all the RKKY components vanish in the insulator phase if u_F is inserted in the energy gap. Similar vanished RKKY interaction has already been discussed in the phosphorene [29].

In addition to the various phases mentioned above, the phase boundary ($k_A = k_c$) between the WSM and the WHM attracts us due to its peculiar dispersion, whose shape is highly spin dependent. As shown in Fig. 2(e), the spin-up band around the Weyl points is linear in all directions. Remarkably different from this, the spin-down band is linear in k_x (or k_y) axis but disperses quadratically in k_z axis, i.e., exhibiting a S-DSM-type dispersion. Since the RKKY interaction is sensitive to the shape of the band structure, thus the magnetic signals characterizing the phase boundary are expected.

To verify the phase transitions shown in Fig. 2, one can calculate the spin-dependent Hall conductivity ζ_{xy}^s. Following the calculation processes in Refs. [9,30], one can obtain $\zeta_{xy}^s = sk_{0,s}e^2/\pi h$. In this way, one can find a net zero Hall conductivity in the DSM due to $\zeta_{xy}^+ = -\zeta_{xy}^-$. Differently, a finite Hall conductivity is obtained in the WSM since ζ_{xy}^+ and ζ_{xy}^- are opposite in sign and unequal in amplitude. More interestingly, a pure spin current can be induced in the WHM due to the vanished ζ_{xy}^- and survived ζ_{xy}^+. As a result, different phases can be distinguished.

Unlike traditional electrical methods in characterizing different phases, we attempt to build the relationship between the magnetic signals and the phase transitions in this work. To construct a model for the indirect magnetic interaction (i.e., the RKKY interaction), two impurities are assumed to be embedded in the bulk of the material. One impurity is located at $\mathbf{r}_1$ and the other is at $\mathbf{r}_2$. Each impurity would interact with the electrons of host material in a contact interaction $H_{\text{int}} = J\mathbf{S}^i \cdot \sigma\delta(\mathbf{r} - \mathbf{r}_i)$, where $\mathbf{S}^i$ ($i = 1$ or 2) denotes the spin of impurity. The two impurities would couple indirectly with each other by the itinerant electrons, thus an effective indirect exchange interaction is generated between two impurities. Using the standard perturbation theory [31–34] by keeping J to the second-order term, the effective exchange interaction

between impurities is given by

$$H_{\mathrm{R}} = -\frac{J^2}{\pi}\mathrm{Im}\int_{-\infty}^{u_F}\mathrm{Tr}[(\mathbf{S}^1\cdot\sigma)G(\omega,\mathbf{R})(\mathbf{S}^2\cdot\sigma)\times G(\omega,-\mathbf{R})]d\omega, \tag{4}$$

where zero temperature is considered and $G(\omega,\mathbf{R})$ is the retarded Green's function with $\mathbf{R}=\mathbf{r}_1-\mathbf{r}_2$.

Before evaluating the RKKY interaction, the retarded Green's functions of real space have to be derived. Using the system Hamiltonian $H(\mathbf{k})$, the retarded Green's function $G(\omega,\mathbf{R})$ can be constructed in Lehmann's representation and it reads as

$$G(\omega,\mathbf{R}) = \frac{1}{(2\pi)^3}\int e^{i\mathbf{k}\mathbf{R}}\frac{1}{\omega+i0^+-H(\mathbf{k})}d^3\mathbf{k}. \tag{5}$$

Inserting the Hamiltonian $H(\mathbf{k})$ of Eq. (1) into the above equation, one can obtain

$$G(\omega,\pm\mathbf{R}) = \begin{pmatrix} G_+(\omega,\pm\mathbf{R}) & \mathbf{0} \\ \mathbf{0} & G_-(\omega,\pm\mathbf{R})\end{pmatrix} \tag{6}$$

with

$$G_s(\omega,\pm\mathbf{R}) = \frac{1}{(2\pi)^3}\int d^3\mathbf{k}e^{i\mathbf{k}\mathbf{R}}\frac{\omega_+-\epsilon_0(\mathbf{k})+\mathbf{h}_s(\mathbf{k})\cdot\tau}{[\omega_+-\epsilon_0(\mathbf{k})]^2-h_s^2(\mathbf{k})}, \tag{7}$$

where $\omega_+=\omega+i0^+$ and $h_s(\mathbf{k})=|\mathbf{h}_s(\mathbf{k})|$. Since the Hamiltonian $H(\mathbf{k})$ of Eq. (1) is diagonal in spin space, the retarded Green's function can also be expressed as a diagonal form in Eq. (6). Inserting the expressions of $\epsilon_0(\mathbf{k})$ and $\mathbf{h}_s(\mathbf{k})$ [Eq. (2)] into the above equation and integrating out the momentum k_z and the angle φ [$\tan(\varphi)=k_y/k_x$], $G_s(\omega,\pm\mathbf{R})$ ($s=\pm$) can be calculated as

$$G_s(\pm\mathbf{R},\omega) = \begin{pmatrix} r_s+t_s & \pm s e^{is\varphi_R}q_s \\ \pm s e^{-is\varphi_R}q_s & r_s-t_s\end{pmatrix}, \tag{8}$$

where $\varphi_R=\arctan(R_y/R_x)$. r_s, t_s, and q_s are given by

$$\begin{aligned} r_s &= \int_0^\infty\left(\omega' f_s + C_1\frac{d^2 f_s}{dR_z^2}\right)\frac{k_\parallel J_0(k_\parallel R_\parallel)}{4\pi\left(C_1^2-M_1^2\right)(g_{s,+}-g_{s,-})}dk_\parallel,\\ t_s &= \int_0^\infty\left(M_s f_s + M_1\frac{d^2 f_s}{dR_z^2}\right)\frac{k_\parallel J_0(k_\parallel R_\parallel)}{4\pi\left(C_1^2-M_1^2\right)(g_{s,+}-g_{s,-})}dk_\parallel,\\ q_s &= \int_0^\infty\frac{i v_s f_s k_\parallel^2 J_1(k_\parallel R_\parallel)}{4\pi\left(C_1^2-M_1^2\right)(g_{s,+}-g_{s,-})}dk_\parallel, \end{aligned} \tag{9}$$

where

$$\begin{aligned} f_s &= \frac{e^{-\sqrt{g_{s,-}}R_z}}{\sqrt{g_{s,-}}}-\frac{e^{-\sqrt{g_{s,+}}R_z}}{\sqrt{g_{s,+}}},\\ \omega' &= \omega_+ - C_0' - C_2 k_\parallel^2,\\ M_s &= M_0' - M_2 k_\parallel^2 - s\lambda,\\ g_{s,\pm} &= \frac{M_s M_1-\omega' C_1}{C_1^2-M_1^2}\pm\sqrt{\frac{(\omega' M_1 - M_s C_1)^2}{\left(C_1^2-M_1^2\right)^2}+\frac{v_s^2 k_\parallel^2}{C_1^2-M_1^2}}. \end{aligned} \tag{10}$$

In Eq. (9), $J_v(x)$ is the nth-order Bessel function of the first kind.

Inserting the Eqs. (6) and (8) into the Eq. (4) and canceling the spin and orbital degrees of freedom, the RKKY interaction H_{R} can be split into the following components,

$$H_{\mathrm{R}} = \sum_{i=x,y} J_{ii}S_i^1 S_i^2 + J_{zz}S_z^1 S_z^2 \tag{11}$$

with

$$\begin{aligned} J_{xx,yy} &= \frac{-4J^2}{\pi}\mathrm{Im}\int_{-\infty}^{u_F}[r_+r_- + t_+t_- + q_-q_+\cos(2\varphi_R)]d\omega,\\ J_{zz} &= \frac{-2J^2}{\pi}\mathrm{Im}\int_{-\infty}^{u_F}(t_+^2+r_+^2-q_+^2+t_-^2+r_-^2-q_-^2)d\omega. \end{aligned} \tag{12}$$

Noting that the subscript $s=\pm$ for r_s, t_s, and q_s refers to the spin of the electrons. Thus, one can find that J_{xx} is induced by the interplay between spin-up and spin-down bands while J_{zz} stems from the contribution of bands with the same spin. Due to the protected inversion symmetry of the Hamiltonian $H(\mathbf{k})$, no DM term arises in Eq. (11), the same result is also found in Ref. [35]. Since $J_{xx}=J_{yy}$ always stands, the RKKY interaction of Eq. (11) can be expressed in another form, which is given by

$$H_{\mathrm{R}} = J_H\mathbf{S}^1\cdot\mathbf{S}^2 + J_I S_z^1 S_z^2 \tag{13}$$

with

$$\begin{aligned} J_H &= J_{xx},\\ J_I &= J_{zz}-J_{xx}, \end{aligned} \tag{14}$$

where J_H is the Heisenberg term and J_I is the Ising term.

III. RKKY SIGNALS CHARACTERIZING THE TOPOLOGICAL PHASES IN THE ABSENCE OF $\epsilon_0(\mathbf{k})$

In this section, we calculate the RKKY interaction in the absence of the term $\epsilon_0(\mathbf{k})$. The effect of $\epsilon_0(\mathbf{k})$ on the RKKY interaction would be discussed in the next section.

A. Case with impurities deposited on z axis

In this section, we focus on the case with impurities deposited on z axis (i.e., the line connecting the Weyl points). In this impurity configuration, one can find $q_\pm=0$ by checking the Eq. (9), where $J_1(k_\parallel R_\parallel)=0$ for the case of $R_\parallel=0$. Plugging r_s and t_s [Eqs. (9)–(10)] into the Eq. (12), the RKKY interaction of zero Fermi energy ($u_F=0$) can be calculated numerically. To carry out the discussion, the RKKY components J_H and J_I versus the light intensity k_A are plotted. According to the Fig. 3, it is found that the RKKY components exhibit significantly different behaviors in different phases, as described below:

(1) In the DSM ($k_A=0$), there only exists the Heisenberg term J_H, which supports an isotropic XXX ($J_{xx}=J_{yy}=J_{zz}$) spin model for the impurities. The same result has also been reported in Refs. [35,36]. For the vanished J_I in the DSM, the related mechanism is attributed to the spin degeneracy under the protection of the TRS. It can be further understood by checking the Eqs. (9)–(10) and (12), where $r_+=r_-$ and $t_+=t_-$ (the subscripts $\pm$ for spin up and down) lead to $J_{xx,yy}=J_{zz}$;

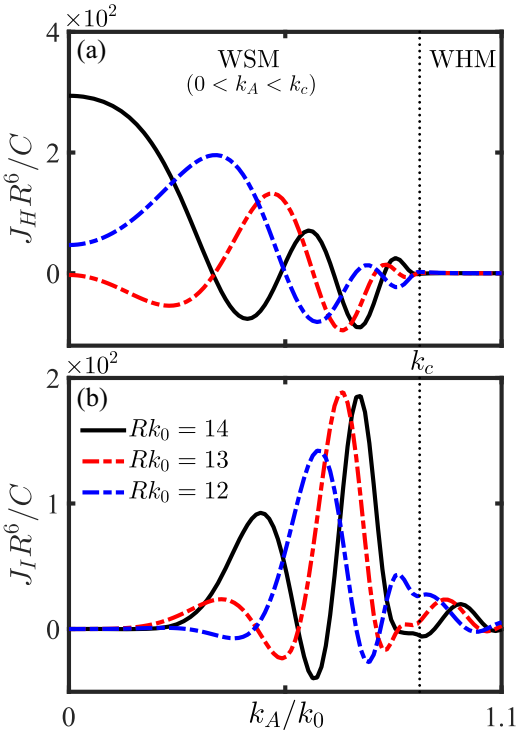

FIG. 3. The RKKY components (a) J_H and (b) J_I versus the light intensity k_A with different impurity distances. Impurities are deposited on the z axis, $u_F = 0$ and $C = J^2/(2\pi)^3$. The vertical dotted lines denote the phase boundary ($k_A = k_c$) between the WSM and the WHM.

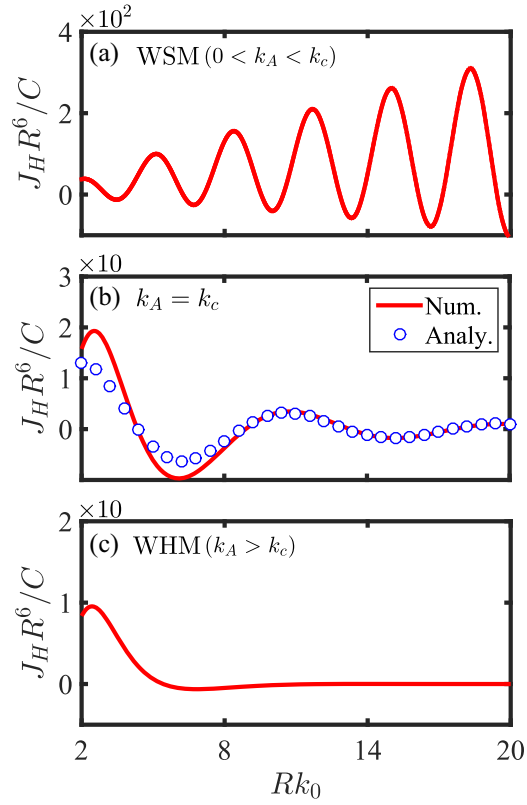

FIG. 4. Spatial dependence of J_H with (a) $k_A = 0.37k_c$ in the WSM ($0 < k_A < k_c$), (b) $k_A = k_c$, and (c) $k_A = 1.18k_c$ in the WHM. The hollow circles in (b) denote the analytical result of the Eq. (B10) in the Appendix B, and the solid lines in (a)–(c) refer to the numerical results calculated from Eqs. (9)–(10), (12), (14).

(2) In the WSM ($0 < k_A < k_c$), a nonzero Ising term J_I arises ($J_I = J_{zz} - J_{xx} \neq 0$) due to the broken spin degeneracy. In this scenario, J_I coexists with J_H. As a result, an anisotropic XXZ spin model ($J_{xx} = J_{yy} \neq J_{zz}$) is generated, which is different from the original isotropic spin model in the DSM;

(3) For the WHM ($k_A > k_c$), it acts like a filter, i.e., J_I still survives but J_H is filtered out once the system is transformed from the WSM to the WHM. As far as we know, this magnetic filtering effect is unique to the WHM, which distinguishes the WHM from the other three-dimensional (3D) materials. Physically, this effect is a reflection of the fully spin-polarized property (i.e., one spin band is in the insulator phase while the other is in the WSM phase). More specifically, the gapped band leads to the vanished J_H while finite J_I is mainly contributed by the WSM-type band. Further explanations are organized as:

(1) To explain the vanished J_H in the WHM, one have to study the decaying law of J_H, since the amplitude of the interaction is mainly determined by the decaying law. We plot the R-dependent J_H with different k_A in Fig. 4. In the WHM [Fig. 4(c)], there arises an exponential decaying law $J_H \propto e^{-\kappa_z^0 R}$ ($\kappa_z^0 = \sqrt{-E_g/2M_1}$), which decays faster than the cases in the WSM ($k_A < k_c$) and at the phase boundary ($k_A = k_c$). To understand this exponential law, one has to notice that J_H is contributed by the terms r_+r_- and t_+t_- in Eq. (12). Here, r_- and t_- are induced by the spin-down band, whose energy gap E_g makes the solution of k_z to be an imaginary number (i.e., $k_z = i\kappa_z^0$). Thus, $J_H(k_A > k_c) \propto e^{-\kappa_z^0 R}$ is obtained since k_z couples with R in the phase factor e^{ik_zR} of the Green's function [Eq. (5)]. Due to the large value of κ_z^0, $J_H \propto e^{-\kappa_z^0 R}$ vanishes if the long-range case (i.e., relatively large R) is considered. This explains the vanished J_H in the WHM shown in Fig. 3(a).

(2) Different from J_H, $J_I = J_{zz} - J_{xx}$ is mainly contributed by the terms t_+^2 and r_+^2 in Eq. (12), since the other terms related to r_- (or t_-) can be ignored due to the exponential decaying law (as stated in previous paragraph). Noting that t_+^2 and r_+^2 are completely induced by the spin-up WSM-type band, which usually generates a decaying law of $J_I \propto 1/R^5$, similar to the case of Fig. 4(a). Thus, the amplitude of J_I is still considerable in the WHM phase [Fig. 3(a)].

In a brief summary, we obtain $J_H \neq 0, J_I = 0$ for the DSM, $J_{H,I} \neq 0$ for the WSM, and $J_H = 0$, $J_I \neq 0$ for the WHM. Thus, one can identify the phase transition of DSM/WSM by checking the Ising term J_I, and the Heisenberg term J_H can be used to distinguish the WSM from the WHM.

B. Case with impurities placed in a direction deviated from z axis

In practice, due to the limitation in the accuracy of the doping techniques, impurities can not be precisely placed in the z axis. One may wonder whether the magnetic signals of Fig. 3(a) still exist when impurities are placed in a direction deviated from z axis. The polarization angle θ_R [$\tan(\theta_R) =$

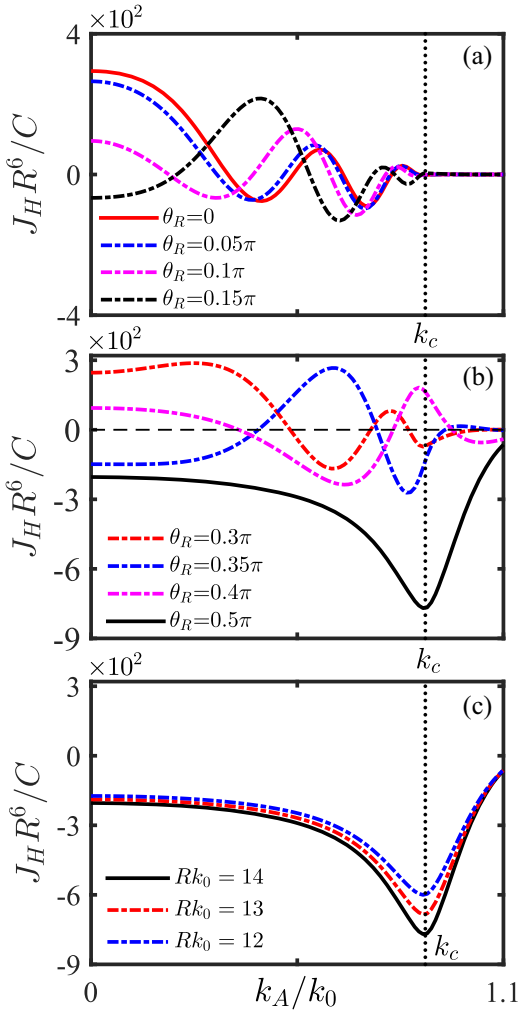

FIG. 5. (a)–(c) The Heisenberg term J_H versus the light intensity k_A with $u_F = 0$ and $\varphi_R = \pi/4$. Here, the vertical dotted lines denote the phase boundary ($k_A = k_c$) between the WSM and the WHM. (a), (b) Different polarization angles θ_R are considered with $Rk_0 = 14$. (c) Impurities are placed in x-y plane (i.e., $\theta_R = \pi/2$) with different impurity distances R.

$R_\parallel/R_z$] is used to evaluate the deviation between the direction of the impurities and the z axis. In the following, we only focus on the Heisenberg term J_H since the signal for the phase transition of DSM/WSM carried by J_I is independent on θ_R.

For a small angle θ_R ($\theta_R \leqslant 0.15\pi$), it is found that J_H still can be used to distinguish the WHM from the WSM, as shown in Fig. 5(a), where the results are similar to the case in Fig. 3(a). In addition, one can also explore the effect of the changed azimuthal angle φ_R on J_H. As shown in Eq. (12), φ_R enters into J_H through a cosine function $\cos(2\varphi_R)$, which only modifies the amplitude of J_H but can not disturb the magnetic signals that characterizes the phase transitions. It is reasonable since the signals are contributed by the different decaying laws of J_H in different phases. If a relatively large θ_R is considered (except $\theta_R = \pi/2$), J_H is failed in characterizing the phase transition of WSM/WHM, as indicated by the dashed lines in Fig. 5(b). The reason is that the original vanished J_H is changed to be a finite one if θ_R increases

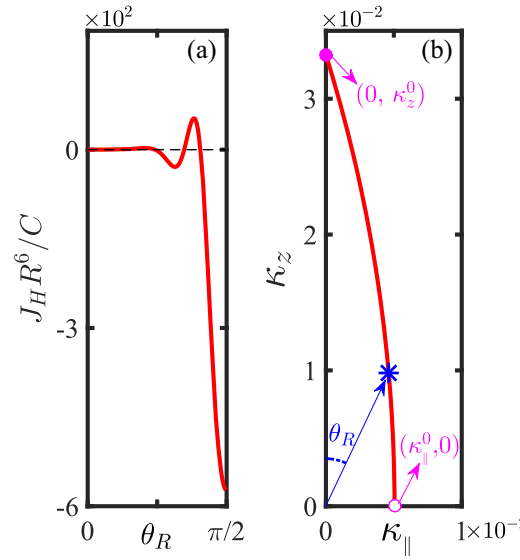

FIG. 6. (a) θ_R-dependent J_H in the WHM phase ($k_A = 0.95k_0$) with $\varphi_R = 0.25\pi$ and $Rk_0 = 14$. (b) The relationship between κ_z and $\kappa_\parallel$. Here, the coordinate system of real space is consistent with that of **k** space. The asterisk denotes the value of $\kappa = \sqrt{\kappa_z^2 + \kappa_\parallel^2}$ taken in the direction of θ_R.

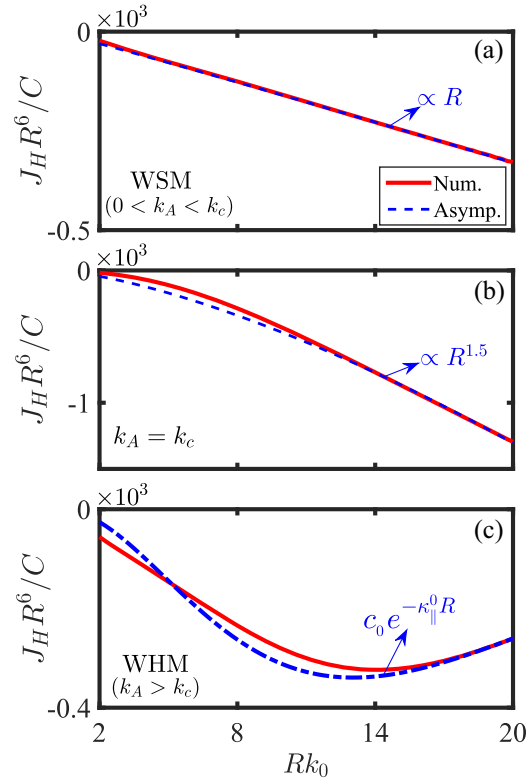

FIG. 7. (a)–(d) Spatial dependence of the Heisenberg term J_H with (a) $k_A = 0.37k_c$ in the WSM ($0 < k_A < k_c$), (b) $k_A = k_c$, and (c) $k_A = 1.24k_c$ in the WHM. The dashed lines denote the long-range asymptotic results for J_H. Here, $c_0 = -0.0165R^{-3.5}$, $\kappa_\parallel^0 = E_g/2v_-$, and $\varphi_R = 0.25\pi$.

substantially, as shown in Fig. 6(a). The high dependence of J_H on θ_R is attributed to the anisotropic imaginary wave number $k = \sqrt{k_z^2 + k_\parallel^2} = i\sqrt{\kappa_z^2 + \kappa_\parallel^2} = i\kappa$, which is induced by the anisotropic gapped spin-down band $E_{-,s'}$. Similar to the case of Fig. 4(c), an exponential decay $J_H \propto e^{-\kappa R}$ is generated. Using the equation $E_{-,s'} = u_F = 0$, the relationship between κ_z and $\kappa_\parallel$ is plotted in Fig. 6(b), where the coordinate system of real space is consistent with that of $\mathbf{k}$ space. In order to make an effective contribution to the RKKY interaction, the value of κ must be taken in the direction of θ_R, as highlighted by an asterisk in Fig. 6(b). According to the Fig. 6(b), one can find $\kappa = \sqrt{(\kappa_z^0)^2 + 0^2} = \kappa_z^0$ for $\theta_R = 0$. In this case, $J_H(\theta_R = 0)$ recovers the result of Fig. 4(c), i.e., $J_H(\theta_R = 0) \propto e^{-\kappa_z^0 R}$. As θ_R changes from 0 to $\pi/2$ (i.e., impurities are moved from z axis to x-y plane), κ decreases dramatically, which brings a great enhancement to the amplitude of J_H because of $J_H \propto e^{-\kappa R}$ $(R > 0)$.

Although the signal of J_H similar to that of Fig. 3(a) is destroyed by the large θ_R, there emerges another signal for J_H to characterize the phase transition of WSM/WHM once the impurities are moved into the x-y plane (i.e., $\theta_R = \pi/2$), as indicated in Figs. 5(b) and 5(c). In the vicinity of the critical point $k_A = k_c$, J_H in the WSM increases with k_A, but it decreases with k_A in the WHM. As a consequence, there emerges a significant dip exactly at $k_A = k_c$, which provides an unambiguous signal to ascertain the phase boundary between the WSM and the WHM. The signal here can also be understood by checking the decaying laws of J_H. According to the long-range asymptotic behaviors of J_H in Fig. 7, one can find a slowest decaying law $J_H \propto 1/R^{4.5}$ at $k_A = k_c$ as compared to the cases in the WSM and the WHM. This law is a result of the interplay between the spin-up Weyl band and the spin-down S-DSM-type band. Noting that the Weyl band contributes a decaying law of $1/R^5$ for the interaction while the S-DSM-type band induces a slowly decaying law of $1/R^4$ [19]. As a result, the interlay of these two bands generates an intermediate decaying law $J_H \propto 1/R^{4.5}$, which is further verified by the analytical result of Eq. (B19) in Appendix B. Due to the slowest decaying law, the largest amplitude of J_H is naturally generated at the phase boundary $(k_A = k_c)$. This explains the dip structure shown in Fig. 5(c).

IV. EFFECT OF $\epsilon_0(\mathbf{k})$ ON THE RKKY SIGNALS

In this section, the effect of $\epsilon_0(\mathbf{k})$ on the RKKY interaction would be discussed. Our ultimate purpose is to test whether the magnetic signals characterizing the phase transitions, as well as the signal for the fully spin-polarized property of the WHM, are still valid.

Before exploring the magnetic signals, we would briefly discuss the effect of $\epsilon_0(\mathbf{k})$ on the band structure, which is plotted in Fig. 8. First, we consider the case of DSM with $k_A = 0$. Due to the broken electron-hole symmetry, $\epsilon_0(\mathbf{k})$ would bring three main effects [Fig. 8(a)], which are organized as: (i) The low-energy bands around the Dirac points are slightly tilted. (ii) An asymmetry between the conduction and valence bands arises, along with the deformed Fermi surface. (iii) The energy bands are lifted as a whole. Once the light intensity k_A is turned on, the effect of (iii) would

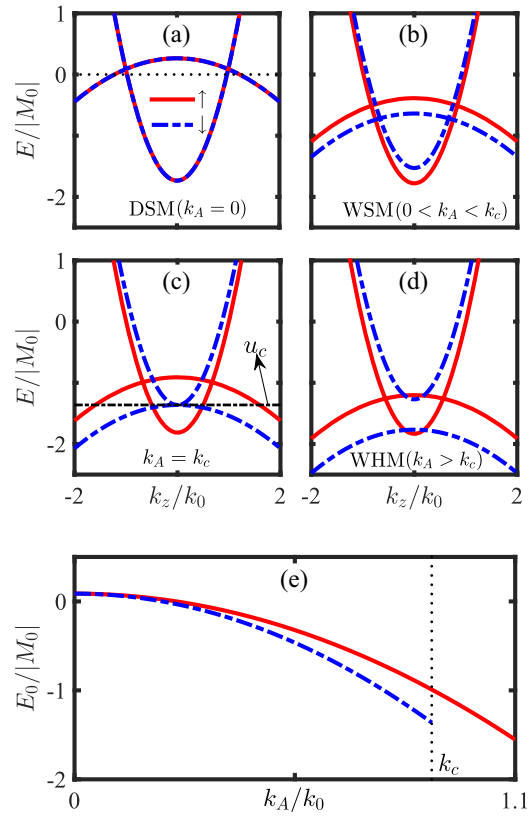

FIG. 8. (a)–(d) Energy dispersion along the k_z axis for different phases in the presence of $\epsilon_0(\mathbf{k})$. Other parameters are the same as that in Figs. 2(a)– 2(d). u_c in (c) refers to the specific Fermi energy at which the spin-down conduction band touches the valence band. (e) The energy of the Weyl points of different spins versus k_A. Parameters $C_0 = -0.06382$ eV, $C_1 = 8.7536$ eV Å^2, $C_2 = -8.4008$ eV Å^2 are extracted from Na_3Bi [27] material.

be substantially modified. As shown in Figs. 8(b)– 8(d), the larger k_A is, the more pronounced is the movement of all energy bands in the negative-energy direction. This movement can also be seen in Fig. 8(e), where the energies of the Weyl points of different spins versus k_A are plotted. Although significant modifications are induced for the energy bands by $\epsilon_0(\mathbf{k})$, the topological phase transitions are undisturbed. Thus, magnetic signals exhibited in previous section are expected to be preserved.

In order to find the survived magnetic signals, one has to display the numerical results of J_H as a function of the Fermi energy u_F, since the bands are drastically shifted in the energy direction as k_A varies. First, the case with impurities deposited on z axis is considered. In Fig. 9(a), we plot $|J_H|$ as a function of u_F and k_A. One can find that the existence of the magnetic signal at $k_A = k_c$ is highly dependent on the selection of the Fermi energy. The signal [the circle in Fig. 9(a)] identifying the phase boundary between the WSM and the WHM can be obtained only in the condition of $u_F = u_c$, which corresponds precisely to the energy of the closing point of the spin-down bands [Fig. 8(c)]. The signal here is similar to that of Fig. 3(a), as verified by the k_A-dependent J_H with the Fermi energy u_c in Fig. 9(b). The survival of the magnetic signal can be

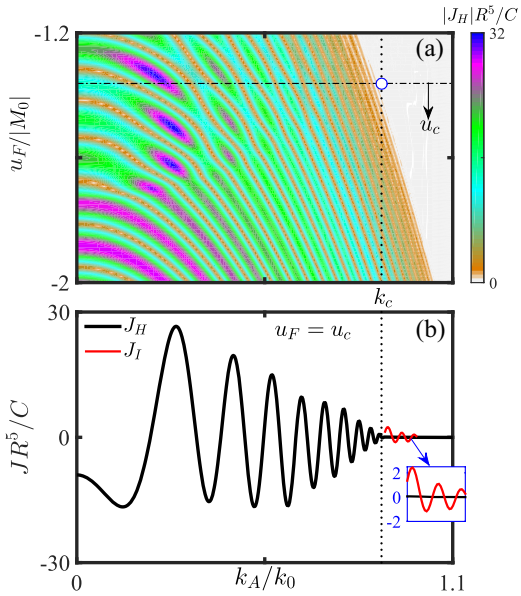

FIG. 9. (a) The Heisenberg term J_H as a function of k_A and u_F. (b) k_A-dependent RKKY components J_H and J_I with $u_F = u_c$. u_c is the specific Fermi energy as depicted in Fig. 8(c), and the red solid line (enlarged in the illustration) refers to the Ising term J_I for a small interval of k_A in the WHM. All results in (a)–(b) are calculated by considering the effect of ϵ_0, and impurities are deposited on z axis with $Rk_0 = 14$.

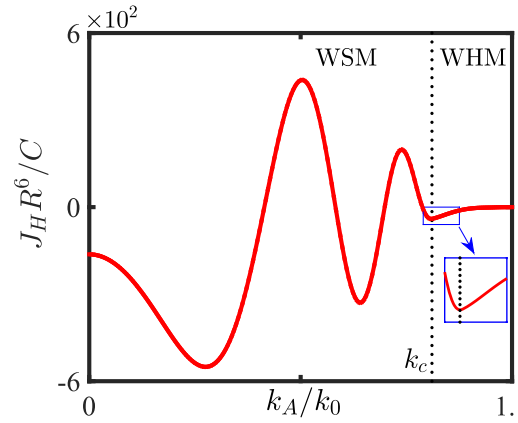

FIG. 10. The Heisenberg term J_H as a function of k_A with $u_F = u_c$ and $Rk_0 = 14$. Here, impurities are placed in x-y plane with $\varphi_R = 0.25\pi$. The vertical dotted lines denote the phase boundary ($k_A = k_c$) between the WSM and the WHM.

understood by reviewing the three effects stated in the previous paragraph. By choosing $u_F = u_c$, the amplitude of J_H around $k_A = k_c$ is only modified by the tilting effect of the band while the other two effects can be ignored. Noting that the magnetic signal here is mainly determined by the decaying laws of the interaction, which can not be changed by the tilting effect of the band [16]. Thus, the magnetic signal still survives in the presence of $\epsilon_0(\mathbf{k})$. In addition, the signal characterizing the fully spin-polarized property also survives, as indicated by the illustration of Fig. 9(b), where $J_H = 0$ and $J_I \neq 0$ in the WHM. Similarly, we plot the k_A-dependent J_H with impurities in x-y plane in Fig. 10, where the Fermi energy is also set as $u_F = u_c$. One can find that there still exists a dip structure for J_H at the phase boundary ($k_A = k_c$).

V. SUMMARY

We have explored the RKKY interaction in Na_3Bi-type DSMs subject to an off-resonant light, which can change the original DSM to the WSM and even to the WHM. It is found that signals can be extracted from the RKKY interaction for characterizing the topological phase transitions. For the phase transition of DSM/WSM, it can be identified by the Ising term J_I, whose existence depends on whether the spin degeneracy of the system is preserved or not. By detecting the Heisenberg term J_H with impurities in the z axis, the phase boundary between the WSM and the WHM can be easily ascertained. In addition, we find that only the Ising term survives in the WHM, which is a reflection of the fully spin-polarized property. For the case with impurities deposited on the x-y plane, the dip structure of J_H can also be used to identify the phase transition of WSM/WHM. Furthermore, we have proved that all magnetic signals are robust to the term that breaks the electron-hole symmetry. Our work has shown that measurement on the RKKY interaction could provide us an alternative method to probe the rich topological phases in 3D Floquet DSMs. Our proposal is feasible with the present techniques, e.g., spin-polarized scanning tunneling spectroscopy [37], which can measure the magnetization curves of individual atoms, or the electron-spin-resonance technique coupled with an optical detection scheme [38,39]. Our results also suggest that the Floquet DSMs are powerful platforms for controlling the magnetic interaction.

ACKNOWLEDGMENTS

This work was supported by the National Natural Science Foundation of China (Grants No. 12104167, No. 12174121, No. 12274146, and No. 11774100), by the Guangdong NSF of China (Grant No. 2024A1515011300), and by Guangdong Basic and Applied Basic Research Foundation (Grants No. 2020A1515111035 and No. 2023B1515020050). S.-M.C., X.W., and Y.-C.C. contributed equally to this work.

APPENDIX A: PHASE TRANSITIONS INDUCED BY THE OFF-RESONANT CPL IN Na_3Bi-TYPE MATERIALS

The model employed in Eq. (1) can be realized by considering the effect of a periodic driving to the following model of DSMs,

$$H_0 = C_0 + C_1 k_z^2 + C_2 k_\parallel^2 + \left(M_0 - M_1 k_z^2 - M_2 k_\parallel^2\right)\tau_z + v_0(k_x\sigma_z\tau_x - k_y\tau_y), \tag{A1}$$

where $k_\parallel^2 = k_x^2 + k_y^2$, $\tau = (\tau_x, \tau_y, \tau_z)$ is the vector of pauli matrix in orbital space, and the subscript $s = +(-)$ for spin up (down). The above model is extracted from the Na_3B_i-type DSMs [27,28]. For the sake of concreteness, a beam of CPL is assumed to be injected in the z axis. The corresponding vector potential is described as $\mathbf{A}(t) = A_0[\cos(\Omega t), \sin(\Omega t), 0]$ with period $T = 2\pi/\Omega$. By applying the Peierls substitution $\mathbf{k} \to \mathbf{k} + e\mathbf{A}/\hbar$, the system Hamiltonian becomes time dependent. Using the Floquet theory [7] with the off-resonant condition of $\hbar\Omega \gg BW$ (BW is the bandwidth), the modified part of the Hamiltonian induced by light reads as

$$H = V_0 + \sum_{n\geqslant 1} \frac{[V_{+n}, V_{-n}]}{n\hbar\Omega} + O\left(\frac{1}{\Omega^2}\right), \tag{A2}$$

where $V_n = \frac{1}{T}\int_0^T H_0(\mathbf{k} + e\mathbf{A}/\hbar)e^{-in\hbar\Omega t}dt$. Specifically, V_0 can be calculated as

$$\begin{aligned} V_0 &= \frac{1}{T}\int_0^T H_0(\mathbf{k} + e\mathbf{A}/\hbar)dt, \\ &= \frac{1}{T}\int_0^T \left\{C_0 + C_1k_z^2 + C_2[k_x + eA_0\cos(\Omega t)/\hbar]^2 + C_2[k_y + eA_0\sin(\Omega t)/\hbar]^2\right\}dt \\ &\quad + \frac{1}{T}\int_0^T \left\{M_0 - M_1k_z^2 - M_2[k_x + eA_0\cos(\Omega t)/\hbar]^2 - M_2[k_y + eA_0\sin(\Omega t)/\hbar]^2\right\}\tau_z dt \\ &\quad + \frac{1}{T}\int_0^T v_0\{[k_x + eA_0\cos(\Omega t)/\hbar]\sigma_z\tau_x - [k_y + eA_0\sin(\Omega t)/\hbar]\tau_y\}dt. \end{aligned} \tag{A3}$$

Noting that $\int_0^T \sin(\Omega t)dt = 0$ and $\int_0^T \cos(\Omega t)dt = 0$, thus the above equation can be further simplified as

$$\begin{aligned} V_0 &= \frac{1}{T}\int_0^T \left[C_0 + C_1k_z^2 + C_2k_\parallel^2 + \left(M_0 - M_1k_z^2 - M_2k_\parallel^2\right)\tau_z + v_0(k_x\sigma_z\tau_x - k_y\tau_y)\right]dt \\ &\quad + \frac{1}{T}\int_0^T \left\{C_2\left[\frac{e^2A_0^2\cos^2(\Omega t)}{\hbar^2} + \frac{e^2A_0^2\sin^2(\Omega t)}{\hbar^2}\right] - M_2\left[\frac{e^2A_0^2\cos^2(\Omega t)}{\hbar^2} + \frac{e^2A_0^2\sin^2(\Omega t)}{\hbar^2}\right]\tau_z\right\}dt, \\ &= H_0 + C_2k_A^2 - M_2k_A^2\tau_z, \end{aligned} \tag{A4}$$

where $k_A = eA_0/\hbar$. As shown above, besides H_0, extra terms $C_2k_A^2$ and $-M_2k_A^2\tau_z$ are generated for V_0. The same extra terms are also found in Refs. [9,13]. Similarly, one can obtain other Floquet sidebands as

$$V_{\pm 1} = \frac{v_0(\sigma_z\tau_x \mp i\tau_y) + 2(k_x \pm ik_y)(C_2 - M_2\tau_z)}{2}k_A, \tag{A5}$$

and $V_n = 0$ for $|n| \geqslant 2$. Substituting the Eqs. (A4)–(A5) into the Eq. (A2), one can obtain the following effective Hamiltonian as

$$H = H_0 + C_2k_A^2 - M_2k_A^2\tau_z - \lambda\sigma_z\tau_z - v_A(k_x\tau_x - k_y\sigma_z\tau_y), \tag{A6}$$

where $\lambda = v_0^2k_A^2/(\hbar\Omega)$ and $v_A = 2v_0k_A^2M_2/(\hbar\Omega)$.

In spin space, the effective Hamiltonian of Eq. (A6) can be rewritten as

$$H = \begin{pmatrix} \epsilon_0(\mathbf{k}) + \mathbf{h}_+(\mathbf{k})\cdot\tau & 0 \\ 0 & \epsilon_0(\mathbf{k}) + \mathbf{h}_-(\mathbf{k})\cdot\tau \end{pmatrix}, \tag{A7}$$

with

$$\begin{aligned} \epsilon_0(\mathbf{k}) &= C_0 + C_2k_A^2 + C_1k_z^2 + C_2k_\parallel^2, \\ \mathbf{h}_s(\mathbf{k}) &= \left(sv_sk_x,\ -v_sk_y,\ M_0 - M_2k_A^2 - M_1k_z^2 - M_2k_\parallel^2 - s\lambda\right), \end{aligned} \tag{A8}$$

where $v_s = v_0 - sv_A$. In the above equations, the terms related to k_A describe the effects of the off-resonant light. Specifically, there are two main effects induced by the off-resonant light. One is that the parameters C_0 and M_0 are modified by the new terms $C_2k_A^2$ and $-M_2k_A^2$, respectively. Note that these terms are spin independent and the energy bands of the system are still spin degenerate. Another effect is that new spin-dependent terms $-s\lambda\tau_z - v_A(k_x\tau_x - sk_y\tau_y)$ are generated to destroy the spin degeneracy. As a result, spin-dependent velocities $v_s = v_0 - sv_A$ arise and the positions of Weyl points of different spin exhibit a different response to the light-field parameter k_A.

Here, the driving frequency $\hbar\Omega$ and the bandwidth BW are set as $\hbar\Omega = 2$ eV and $BW = 0.24$ eV. The off-resonant condition is satisfied since $\hbar\Omega \gg BW$. The setting of the bandwidth, as well as the frequency, is reasonable since we only concern the low-energy behavior with the energy in the range of $|E| < 0.12$ eV.

APPENDIX B: DERIVATION OF THE ANALYTICAL RKKY INTERACTION AT THE PHASE BOUNDARY BETWEEN THE WSM AND THE WHM

Here, we drop the term $\epsilon(\mathbf{k})$ for facilitating the calculation of the analytical results. For the phase boundary between the WSM and the WHM, i.e., at the critical point $k_A = k_c = \sqrt{M_0/[M_2 - v_0^2/(\hbar\Omega)]}$, the spin-up band is in the WSM phase while the spin-down one is in the S-DSM phase. For the spin-up band, the bulk conduction and valence bands touch each other at two Weyl points located at $(0, 0, \pm k_{0,+})$ with $k_{0,+} = \sqrt{(M_0 - M_2 k_A^2 - \lambda)/M_1}$. In this case, one can linearize the Hamiltonian H_+ of the Eq. (A7) around the Weyl points $(0, 0, \pm k_{0,+})$ to the following low-energy model:

$$H_{+,\eta} = \begin{pmatrix} \eta v_z k_z' & v_+(k_x + ik_y) \\ v_+(k_x - ik_y) & -\eta v_z k_z' \end{pmatrix}, \tag{B1}$$

where $v_z = -2M_1 k_{0,+}$ and $\eta = \pm$ denote the chirality of the two Weyl points. For the spin-down band, the Hamiltonian H_- in the Eq. (A7) can be further simplified as

$$H_- = \begin{pmatrix} -M_1 k_z^2 & -v_-(k_x - ik_y) \\ -v_-(k_x + ik_y) & M_1 k_z^2 \end{pmatrix}. \tag{B2}$$

1. Case with impurities deposited on the line connecting the Weyl points

For impurities in the z axis [i.e., $\mathbf{R} = (0, 0, R_z)$], according to the Eqs. (5) and (B1), the Green's function of the spin-up band can be calculated as

$$\begin{aligned}
G_+(\mathbf{R}, \omega) &= \sum_{\eta=\pm} \frac{1}{(2\pi)^3} \iiint dk_x dk_y dk_z' e^{i(k_z' + \eta k_{0,+})R_z} \frac{1}{\omega^2 - v_+^2 k_\parallel^2 - v_z^2 k_z'^2} \begin{pmatrix} \omega + \eta v_z k_z' & v_+(k_x + ik_y) \\ v_+(k_x - ik_y) & \omega - \eta v_z k_z' \end{pmatrix}, \\
&= \sum_{\eta=\pm} e^{i\eta k_{0,+} R_z} \frac{1}{(2\pi)^3} \int k_\parallel dk_\parallel \int dk_z' e^{ik_z' R_z} \int_0^{2\pi} d\theta_\parallel \frac{1}{\omega^2 - v_+^2 k_\parallel^2 - v_z^2 k_z'^2} \begin{pmatrix} \omega + \eta v_z k_z' & v_+ k_\parallel e^{i\theta_\parallel} \\ v_+ k_\parallel e^{-i\theta_\parallel} & \omega - \eta v_z k_z' \end{pmatrix}, \\
&= \sum_{\eta=\pm} e^{i\eta k_{0,+} R_z} \frac{2}{(2\pi)^2} \int_0^\infty dk_\parallel \int_0^\infty dk_z' k_\parallel \frac{1}{\omega^2 - v_+^2 k_\parallel^2 - v_z^2 k_z'^2} \\
&\quad \times \begin{pmatrix} \omega \cos(k_z' R_z) + i\eta v_z k_z' \sin(k_z' R_z) & 0 \\ 0 & \omega \cos(k_z' R_z) - i\eta v_z k_z' (k_z' R_z) \end{pmatrix},
\end{aligned} \tag{B3}$$

Applying a parameter transformation $v_+ k_\parallel = v_z k_\parallel'$, the above Green's function can be further simplified as

$$\begin{aligned}
G_+(\mathbf{R}, \omega) &= \sum_{\eta=\pm} e^{i\eta k_{0,+} R_z} \frac{2}{(2\pi)^2} \frac{v_z^2}{v_+^2} \int_0^\infty dk_\parallel' \int_0^\infty dk_z' k_\parallel' \frac{\begin{pmatrix} \omega \cos(k_z' R_z) + i\eta v_z k_z' \sin(k_z' R_z) & 0 \\ 0 & \omega \cos(k_z' R_z) - i\eta v_z k_z' (k_z' R_z) \end{pmatrix}}{\omega^2 - v_z^2 k_\parallel'^2 - v_z^2 k_z'^2}, \\
&= \sum_{\eta=\pm} e^{i\eta k_{0,+} R_z} \frac{2v_z^2}{(2\pi)^2 v_+^2} \int_0^\infty k^2 dk \frac{\begin{pmatrix} \omega \frac{\sin(kR_z)}{kR_z} + i\eta v_z k \frac{\sin(kR_z) - kR_z \cos(kR_z)}{k^2 R_z^2} & 0 \\ 0 & \omega \frac{\sin(kR_z)}{kR_z} - i\eta v_z k \frac{\sin(kR_z) - kR_z \cos(kR_z)}{k^2 R_z^2} \end{pmatrix}}{\omega^2 - v_z^2 k^2}, \\
&= \begin{pmatrix} r_+ + t_+ & 0 \\ 0 & r_+ - t_+ \end{pmatrix},
\end{aligned} \tag{B4}$$

with

$$\begin{aligned}
r_+ &= \frac{-\omega}{2\pi v_+^2} \frac{\cos(k_{0,+} R_z)}{R_z} e^{i\frac{R_z \omega}{v_z}}, \\
t_+ &= -\frac{v_z \sin(k_{0,+} R_z)}{2\pi v_+^2 R_z^2} \left(\frac{i\omega R_z}{v_z} - 1 \right) e^{i\frac{R_z \omega}{v_z}}.
\end{aligned} \tag{B5}$$

Similarly, one can calculate $G_+(-\mathbf{R}, \omega)$, which satisfies $G_+(-\mathbf{R}, \omega) = G_+(\mathbf{R}, \omega)$.

According to the Eqs. (5) and (B2), the Green's function of the spin-down band can be calculated as

$$
\begin{aligned}
G_-(\mathbf{R},\omega) &= \frac{1}{(2\pi)^3}\iiint dk_x dk_y dk_z e^{ik_z R_z}\frac{\begin{pmatrix}\omega - M_1 k_z^2 & -v_-(k_x - ik_y)\\ -v_-(k_x + ik_y) & \omega + M_1 k_z^2\end{pmatrix}}{\omega^2 - v_-^2 k_\parallel^2 - M_1^2 k_z^4},\\
&= \frac{1}{(2\pi)^3}\int_0^\infty k_\parallel dk_\parallel \int dk_z e^{ik_z R_z}\int_0^{2\pi} d\theta_\parallel \frac{\begin{pmatrix}\omega - M_1 k_z^2 & -v_- k_\parallel e^{-i\theta_\parallel}\\ -v_- k_\parallel e^{i\theta_\parallel} & \omega + M_1 k_z^2\end{pmatrix}}{\omega^2 - v_-^2 k_\parallel^2 - M_1^2 k_z^4},\\
&= \frac{2}{(2\pi)^2}\int_0^\infty k_\parallel dk_\parallel \int_0^\infty dk_z \cos(k_z R_z)\frac{\begin{pmatrix}\omega - M_1 k_z^2 & 0\\ 0 & \omega + M_1 k_z^2\end{pmatrix}}{\omega^2 - v_-^2 k_\parallel^2 - M_1^2 k_z^4},\\
&= \frac{1}{4\pi^2}\int_0^\infty dk_\parallel \int_0^\infty dk_z' \frac{k_\parallel \cos(\sqrt{k_z'} R_z)}{\sqrt{k_z'}}\frac{\begin{pmatrix}\omega - M_1 k_z' & 0\\ 0 & \omega + M_1 k_z'\end{pmatrix}}{\omega^2 - v_-^2 k_\parallel^2 - M_1^2 k_z'^2},\\
&= \frac{M_1^2}{4\pi^2 v_-^2}\int_0^\infty dk_\parallel' \int_0^\infty dk_z' \frac{k_\parallel' \cos(\sqrt{k_z'} R_z)}{\sqrt{k_z'}}\frac{\begin{pmatrix}\omega - M_1 k_z' & 0\\ 0 & \omega + M_1 k_z'\end{pmatrix}}{\omega^2 - M_1^2 k_\parallel'^2 - M_1^2 k_z'^2},\\
&= \frac{M_1^2}{4\pi^2 v_-^2}\int_0^\infty \frac{k^{3/2}}{\omega^2 - M_1^2 k^2} dk \int_0^{\frac{\pi}{2}} d\theta \frac{\cos(\theta)\cos[\sqrt{k\sin(\theta)} R_z]}{\sqrt{\sin(\theta)}}\begin{pmatrix}\omega - M_1 k\sin(\theta) & 0\\ 0 & \omega + M_1 k\sin(\theta)\end{pmatrix},\\
&= \frac{M_1^2 \omega}{2\pi^2 v_-^2 R_z}\int_0^\infty \frac{k\sin(\sqrt{k} R_z)}{\omega^2 - M_1^2 k^2} dk \begin{pmatrix}1 & 0\\ 0 & 1\end{pmatrix}\\
&\quad + \frac{M_1^3}{2\pi^2 v_-^2 R_z^3}\int_0^\infty \frac{k\sin(\sqrt{k} R_z)\left(2 - kR_z^2\right) - 2R_z k^{3/2}\cos(\sqrt{k} R_z)}{\omega^2 - M_1^2 k^2} dk \begin{pmatrix}1 & 0\\ 0 & -1\end{pmatrix},\\
&= \begin{pmatrix}r_- + t_- & 0\\ 0 & r_- - t_-\end{pmatrix},
\end{aligned}
\tag{B6}
$$

where

$$
\begin{aligned}
r_- &= -\frac{\omega}{4\pi R_z v_-^2}\left(e^{iR_z\sqrt{\frac{\omega}{-M_1}}} + e^{-R_z\sqrt{\frac{\omega}{-M_1}}}\right),\\
t_- &= e^{iR_z\sqrt{\frac{\omega}{-M_1}}}\frac{-2iR_z\sqrt{-M_1\omega} - R_z^2\omega - 2M_1}{4\pi v_-^2 R_z^3} + e^{-R_z\sqrt{\frac{\omega}{-M_1}}}\frac{2R_z\sqrt{-M_1\omega} + R_z^2\omega - 2M_1}{4\pi v_-^2 R_z^3}.
\end{aligned}
\tag{B7}
$$

Similarly, one can calculate $G_-(-\mathbf{R},\omega)$, which satisfies $G_-(-\mathbf{R},\omega) = G_-(\mathbf{R},\omega)$.

Plugging the Green's functions of Eqs. (B4) and (B6) into the Eq. (4) of the main text and summing over the spin and orbital degrees of freedom, the RKKY components can be written in the form of

$$
H_{\mathrm{R}} = J_{xx}\left(S_1^x S_2^x + S_1^y S_2^y\right) + J_{zz} S_1^z S_2^z,
\tag{B8}
$$

with

$$
\begin{aligned}
J_{xx} &= \frac{-4\lambda^2}{\pi}\mathrm{Im}\int_{-\infty}^0 (r_+ r_- + t_+ t_-) d\omega,\\
J_{zz} &= \frac{-2\lambda^2}{\pi}\mathrm{Im}\int_{-\infty}^0 (r_+^2 + r_-^2 + t_+^2 + t_-^2) d\omega.
\end{aligned}
\tag{B9}
$$

Plugging the Eqs. (B5) and (B7) into the above equation, J_{xx} can be calculated as

$$
\begin{aligned}
J_{xx} &= -\mathrm{Im}\int_{-\infty}^0 d\omega \frac{e^{\frac{iR_z\omega}{v_z}}\left(e^{iR_z\sqrt{\frac{\omega}{-M_1}}} + e^{-R_z\sqrt{\frac{\omega}{-M_1}}}\right)\omega^2}{2\pi^3 R_z^2 v_-^2 v_+^2/[\lambda^2\cos(k_{0,+}R_z)]} - \mathrm{Im}\int_{-\infty}^0 d\omega \frac{e^{R_z(\frac{i\omega}{v_z} - \sqrt{\frac{\omega}{-M_1}})}(v_z - iR_z\omega)[R_z(R_z\omega + 2\sqrt{-M_1\omega}) - 2M_1]}{2\pi^3 R_z^5 v_-^2 v_+^2/[\lambda^2\sin(k_0 R_z)]}\\
&\quad + \mathrm{Im}\int_{-\infty}^0 d\omega \frac{e^{iR_z(\frac{\omega}{v_z} + \sqrt{\frac{\omega}{-M_1}})}(v_z - iR_z\omega)[R_z(R_z\omega + i2\sqrt{-M_1\omega}) + 2M_1]}{2\pi^3 R_z^5 v_-^2 v_+^2/[\lambda^2\sin(k_0 R_z)]},\\
&= \frac{\left(R_z^3 v_z^3 - 32M_1^2 R_z v_z\right)\cot(k_0 R_z) + 2M_1\left(9v_z^2 R_z^2 - 32M_1^2\right)}{16\pi^3 M_1^2 R_z^6 v_-^2 v_+^2/\left[v_z^2\sin(k_0 R_z)\right]}
\end{aligned}
$$

$$+\mathrm{Im}\left\{\frac{(1+i)e^{-\frac{iR_zv_z}{4M_1}}\left(v_z^2R_z^2-60M_1^2+i20M_1R_zv_z\right)\mathrm{erfc}\left[\frac{(-1)^{1/4}\sqrt{R_zv_z}}{2\sqrt{-M_1}}\right]}{64\sqrt{2}M_1^{5/2}\pi^{5/2}R_z^{9/2}v_-^2v_+^2/\left[v_z^{7/2}\cos\left(k_0R_z\right)\right]}\right\}$$

$$+\mathrm{Im}\left\{\frac{(1-i)e^{-\frac{iR_zv_z}{4M_1}}\left(v_z^2R_z^2-28M_1^2+i20M_1R_zv_z\right)\mathrm{erfc}\left[\frac{(-1)^{1/4}\sqrt{R_zv_z}}{2\sqrt{-M_1}}\right]+(1+i)e^{\frac{iR_zv_z}{4M_1}}\left(v_z^2R_z^2-28M_1^2-i20M_1R_zv_z\right)\mathrm{erfc}\left[\frac{(-1)^{3/4}\sqrt{R_zv_z}}{-2\sqrt{-M_1}}\right]}{64\sqrt{2}M_1^{5/2}\pi^{5/2}R_z^{9/2}v_-^2v_+^2/\left[v_z^{7/2}\sin\left(k_0R_z\right)\right]}\right\}$$

$$-\mathrm{Im}\left\{\frac{(1-i)e^{\frac{iR_zv_z}{4M_1}}\left(60M_1^2+i20M_1R_zv_z-v_z^2R_z^2\right)\mathrm{erfc}\left[\frac{(-1)^{3/4}\sqrt{R_zv_z}}{-2\sqrt{-M_1}}\right]}{64\sqrt{2}M_1^{5/2}\pi^{5/2}R_z^{9/2}v_-^2v_+^2/\left[v_z^{7/2}\cos\left(k_0R_z\right)\right]}\right\}, \tag{B10}$$

where $\mathrm{erfc}(t)$ is the complementary error function. Similarly, J_{zz} can be calculated as

$$\begin{aligned}J_{zz}&=\mathrm{Im}\int_{-\infty}^{0}e^{\frac{i2R_z\omega}{v_z}}\frac{[v_z-(1+i)R_z\omega][v_z+(1-i)R_z\omega]\cos\left(2k_{0,+}R_z\right)-v_z(v_z-i2R_z\omega)}{4\pi^3R_z^4v_+^4}d\omega\\&\quad-\mathrm{Im}\int_{-\infty}^{0}\frac{\left(e^{iR_z\sqrt{\frac{\omega}{-M_1}}}+e^{-R_z\sqrt{\frac{\omega}{-M_1}}}\right)^2\omega^2}{8\pi^3R_z^2v_-^4}d\omega\\&\quad-\mathrm{Im}\int_{-\infty}^{0}\frac{\left[e^{-R_z\sqrt{\frac{\omega}{-M_1}}}\left(2R_z\sqrt{-M_1\omega}+R_z^2\omega-2M_1\right)-e^{iR_z\sqrt{\frac{\omega}{-M_1}}}\left(2iR_z\sqrt{-M_1\omega}+R_z^2\omega+2M_1\right)\right]^2}{8\pi^3R_z^6v_-^4}d\omega,\\&=\frac{v_z^3[2-3\cos\left(2k_{0,+}R_z\right)]}{8\pi^3R_z^5v_+^4}-\frac{12M_1^3}{\pi^3R_z^8v_-^4}.\end{aligned} \tag{B11}$$

2. Case with impurities deposited on the plane perpendicular to the line connecting the Weyl points

For impurities deposited on the x-y plane [i.e., $\mathbf{R}=(R_x,R_y,0)$], according to the Eqs. (5) and (B1), the Green's function of the spin-up band can be calculated as

$$\begin{aligned}G_+(\mathbf{R},\omega)&=\sum_{\eta=\pm}\frac{1}{(2\pi)^3}\iiint dk_xdk_ydk_z'e^{i\left(k_xR_x+k_yR_y\right)}\frac{1}{\omega^2-v_+^2k_\parallel^2-v_z^2k_z'^2}\begin{pmatrix}\omega+\eta v_zk_z' & v_+(k_x+ik_y)\\ v_+(k_x-ik_y) & \omega-\eta v_zk_z'\end{pmatrix},\\&=\frac{1}{2\pi^3}\int_0^\infty k_\parallel dk_\parallel\int_0^\infty dk_z'\int_0^{2\pi}d\varphi e^{ik_\parallel R_\parallel\cos\left(\varphi-\varphi_R\right)}\frac{1}{\omega^2-v_+^2k_\parallel^2-v_z^2k_z'^2}\begin{pmatrix}\omega & v_+k_\parallel e^{i\varphi}\\ v_+k_\parallel e^{-i\varphi} & \omega\end{pmatrix},\\&=\frac{1}{\pi^2}\int_0^\infty k_\parallel dk_\parallel\int_0^\infty dk_z'\frac{1}{\omega^2-v_+^2k_\parallel^2-v_z^2k_z'^2}\begin{pmatrix}\omega J_0(k_\parallel R_\parallel) & v_+ie^{i\varphi_R}k_\parallel J_1(k_\parallel R_\parallel)\\ v_+ie^{-i\varphi_R}k_\parallel J_1(k_\parallel R_\parallel) & \omega J_0(k_\parallel R_\parallel)\end{pmatrix},\end{aligned} \tag{B12}$$

where $\varphi_R=\arctan(R_y/R_x)$. Applying a parameter transformation $v_zk_z'=v_+k_z$, the above Green's function can be further simplified as

$$\begin{aligned}G_+(\mathbf{R},\omega)&=\frac{v_+}{\pi^2v_z}\int_0^\infty k_\parallel dk_\parallel\int_0^\infty dk_z\frac{1}{\omega^2-v_+^2k_\parallel^2-v_+^2k_z^2}\begin{pmatrix}\omega J_0(k_\parallel R_\parallel) & v_+ie^{i\varphi_R}k_\parallel J_1(k_\parallel R_\parallel)\\ v_+ie^{-i\varphi_R}k_\parallel J_1(k_\parallel R_\parallel) & \omega J_0(k_\parallel R_\parallel)\end{pmatrix},\\&=\frac{v_+}{\pi^2v_z}\int_0^\infty\frac{k^2}{\omega^2-v_+^2k^2}dk\int_0^{\frac{\pi}{2}}d\theta\cos\left(\theta\right)\begin{pmatrix}\omega J_0[kR_\parallel\cos\left(\theta\right)] & v_+ie^{i\varphi_R}k\cos\left(\theta\right)J_1[kR_\parallel\cos\left(\theta\right)]\\ v_+ie^{-i\varphi_R}k\cos\left(\theta\right)J_1[kR_\parallel\cos\left(\theta\right)] & \omega J_0[kR_\parallel\cos\left(\theta\right)]\end{pmatrix},\\&=\frac{v_+}{\pi^2v_zR_\parallel}\int_0^\infty\frac{k}{\omega^2-v_+^2k^2}dk\begin{pmatrix}\omega\sin(kR_\parallel) & v_+ie^{i\varphi_R}[\sin(kR_\parallel)/R_\parallel-k\cos(kR_\parallel)]\\ v_+ie^{-i\varphi_R}[\sin(kR_\parallel)/R_\parallel-k\cos(kR_\parallel)] & \omega\sin(kR_\parallel)\end{pmatrix},\\&=\begin{pmatrix}r_+ & e^{i\varphi_\parallel}q_+\\ e^{-i\varphi_\parallel}q_+ & r_+\end{pmatrix},\end{aligned} \tag{B13}$$

where

$$r_+=-\frac{\omega}{2\pi v_+v_zR_\parallel}e^{i\frac{\omega R_\parallel}{v_+}},\qquad q_+=-\frac{iv_++\omega R_\parallel}{2\pi v_+v_zR_\parallel^2}e^{i\frac{\omega R_\parallel}{v_+}}. \tag{B14}$$

Similarly, one can calculate $G_+(-\mathbf{R},\omega)$, which satisfies $G_+(-\mathbf{R},\omega)=G_+(\mathbf{R},\omega)|_{q_+\to-q_+}$.

According to the Eqs. (5) and (B2), the Green's function of the spin-down band can be calculated as

$$\begin{aligned}
G_-(\mathbf{R},\omega) &= \frac{1}{(2\pi)^3}\iint dk_x dk_y \int dk_z e^{i(k_x R_x + k_y R_y)} \frac{\begin{pmatrix} \omega - M_1 k_z^2 & -v_-(k_x - ik_y) \\ -v_-(k_x + ik_y) & \omega + M_1 k_z^2 \end{pmatrix}}{\omega^2 - v_-^2 k_\parallel^2 - M_1^2 k_z^4}, \\
&= \frac{1}{(2\pi)^3}\int_0^\infty k_\parallel dk_\parallel \int dk_z \int_0^{2\pi} d\varphi e^{ik_\parallel R_\parallel \cos(\varphi-\varphi_R)} \frac{\begin{pmatrix} \omega - M_1 k_z^2 & -v_- k_\parallel e^{-i\varphi} \\ -v_- k_\parallel e^{i\varphi} & \omega + M_1 k_z^2 \end{pmatrix}}{\omega^2 - v_-^2 k_\parallel^2 - M_1^2 k_z^4}, \\
&= \frac{2}{(2\pi)^2}\int_0^\infty k_\parallel dk_\parallel \int_0^\infty dk_z \frac{\begin{pmatrix} (\omega - M_1 k_z^2) J_0(k_\parallel R_\parallel) & -v_- i e^{-i\varphi_R} k_\parallel J_1(k_\parallel R_\parallel) \\ -v_- i e^{i\varphi_R} k_\parallel J_1(k_\parallel R_\parallel) & (\omega + M_1 k_z^2) J_0(k_\parallel R_\parallel) \end{pmatrix}}{\omega^2 - v_-^2 k_\parallel^2 - M_1^2 k_z^4}.
\end{aligned} \tag{B15}$$

Applying a parameter transformation $-M_1 k_z^2 = v_- k_z'$, the above Green's function can be further simplified as

$$\begin{aligned}
G_-(\mathbf{R},\omega) &= \frac{\sqrt{v_-}}{(2\pi)^2\sqrt{-M_1}}\int_0^\infty k_\parallel dk_\parallel \int_0^\infty dk_z' \frac{1}{\sqrt{k_z'}} \frac{\begin{pmatrix} (\omega + v_- k_z') J_0(k_\parallel R_\parallel) & -v_- i e^{-i\varphi_R} k_\parallel J_1(k_\parallel R_\parallel) \\ -v_- i e^{i\varphi_R} k_\parallel J_1(k_\parallel R_\parallel) & (\omega - v_- k_z') J_0(k_\parallel R_\parallel) \end{pmatrix}}{\omega^2 - v_-^2 k_\parallel^2 - v_-^2 k_z'^2}, \\
&= \frac{\sqrt{v_-}}{(2\pi)^2\sqrt{-M_1}}\int_0^\infty k^{3/2} dk \int_0^{\frac{\pi}{2}} d\theta \frac{\cos(\theta)}{\sqrt{\sin(\theta)}} \frac{\begin{pmatrix} [\omega + v_- k\sin(\theta)] J_0[k\cos(\theta) R_\parallel] & -v_- i e^{-i\varphi_R} k\cos(\theta) J_1[k\cos(\theta) R_\parallel] \\ -v_- i e^{i\varphi_R} k\cos(\theta) J_1[k\cos(\theta) R_\parallel] & [\omega - v_- k\sin(\theta)] J_0[k\cos(\theta) R_\parallel] \end{pmatrix}}{\omega^2 - v_-^2 k^2}, \\
&= \frac{\sqrt{v_-}}{2\pi^2\sqrt{-M_1}}\int_0^\infty \frac{k^{3/2}}{\omega^2 - v_-^2 k^2} \begin{pmatrix} {}_0F_1\left(;\frac{5}{4};-\frac{k^2R_\parallel^2}{4}\right)\omega + \frac{{}_0F_1\left(;\frac{7}{4};-\frac{k^2R_\parallel^2}{4}\right)v_- k}{3} & -2v_- i e^{-i\varphi_R} R_\parallel \frac{{}_0F_1\left(;\frac{9}{4};-\frac{k^2R_\parallel^2}{4}\right)k^2}{5} \\ -2v_- i e^{i\varphi_R} R_\parallel \frac{{}_0F_1\left(;\frac{9}{4};-\frac{k^2R_\parallel^2}{4}\right)k^2}{5} & {}_0F_1\left(;\frac{5}{4};-\frac{k^2R_\parallel^2}{4}\right)\omega - \frac{{}_0F_1\left(;\frac{7}{4};-\frac{k^2R_\parallel^2}{4}\right)v_- k}{3} \end{pmatrix} dk, \\
&= \begin{pmatrix} r_- + t_- & -e^{-i\varphi_R} q_- \\ -e^{i\varphi_R} q_- & r_- - t_- \end{pmatrix}.
\end{aligned} \tag{B16}$$

In the above equation, ${}_0F_1(;b;t)$ is the confluent hypergeometric function, and r_-, t_-, q_- read as

$$\begin{aligned}
r_- &= \frac{(-1)^{7/8}\sqrt{-v_-/M_1}\,\omega^{5/4} K_{1/4}(-iR_\parallel\omega/v_-)\Gamma(5/4)}{2^{3/4}\pi^2 v_-^{9/4} R_\parallel^{1/4}}, \\
t_- &= \frac{(-1)^{5/8}\omega^{3/4} K_{3/4}(-iR_\parallel\omega/v_-)\Gamma(7/4)}{3\times 2^{1/4}\sqrt{-M_1}\pi^2 v_-^{5/4} R_\parallel^{3/4}}, \\
q_- &= -\frac{\omega^{5/4} K_{5/4}(-iR_\parallel\omega/v_-)\Gamma(5/4)}{(1-i)^{3/2} M_1^{1/2}\pi^2 v_-^{7/4} R_\parallel^{1/4}},
\end{aligned} \tag{B17}$$

where $K_v(t)$ is the modified Bessel function of the second kind and $\Gamma(t)$ is the Gamma function. Similarly, one can calculate $G_-(-\mathbf{R},\omega)$, which satisfies $G_-(-\mathbf{R},\omega) = G_-(\mathbf{R},\omega)|_{q_-\to -q_-}$.

Plugging the Green's function of Eqs. (B13) and (B16) into the Eq. (4) of the main text and summing over the spin and orbital degrees of freedom, the RKKY components can be written as $H_{\mathrm{R}} = J_{xx}(S_1^x S_2^x + S_1^y S_2^y) + J_{zz} S_1^z S_2^z$, where J_{xx} and J_{zz} read as

$$\begin{aligned}
J_{xx} &= \frac{-4\lambda^2}{\pi}\mathrm{Im}\int_{-\infty}^{u_F} [r_+ r_- + q_- q_+ \cos(2\varphi_R)] d\omega, \\
J_{zz} &= \frac{-2\lambda^2}{\pi}\mathrm{Im}\int_{-\infty}^{u_F} (r_+^2 - q_+^2 + t_-^2 + r_-^2 - q_-^2) d\omega.
\end{aligned} \tag{B18}$$

Plugging the Eqs. (B14) and (B17) to the RKKY component J_{xx} of the above equation, J_{xx} can be solved as

$$\begin{aligned}
J_{xx} &= -\mathrm{Im}\int_{-\infty}^{0} e^{\frac{iR_\parallel\omega}{v_+}}\frac{\lambda^2\Gamma(5/4)\omega^{5/4}\sqrt{1-i}}{\pi^4 R_\parallel^{5/4}v_-^{7/4}v_+v_z\sqrt{-M_1}}\left[\omega K_{1/4}(-iR_\parallel\omega/v_-)+\frac{(iv_++R_\parallel\omega)K_{5/4}(-iR_\parallel\omega/v_-)\cos(2\varphi_R)}{R_\parallel}\right]d\omega,\\
&= \frac{1}{R_\parallel^{4.5}}\frac{1024\sqrt{\pi}v_+^{7/2}(v_+^2-v_-^2)^{1/4}(5v_-^2+2v_+^2)\Gamma(2.75)+1575(v_-^2-v_+^2)^3\Gamma(-3.75)\left[{}_2F_1\left(3,3.5;3.75;\frac{v_++v_-}{2v_+}\right)\right]}{896\sqrt{2}\pi^4M_1v_+(v_+^2-v_-^2)^3v_z/[\lambda^2\sqrt{-M_1}v_-^{3/2}\Gamma(1.25)]}\\
&\quad+\frac{1}{R_\parallel^{4.5}}\frac{1024\sqrt{\pi}v_+^{9/2}(v_+^2-v_-^2)^{1/4}(2v_+^2-9v_-^2)\Gamma(1.75)+225(v_-^2-v_+^2)^3\Gamma(-3.75)}{512\sqrt{2}\pi^4\sqrt{-M_1}(v_-^2-v_+^2)^3v_+v_z/[\sqrt{v_-}\Gamma(1.25)]}\cos(2\varphi_R)\\
&\quad+\frac{1}{R_\parallel^{4.5}}\frac{11v_+\left[{}_2F_1\left(1,3.5;2.75;\frac{v_-+v_+}{2v_+}\right)\right]-7v_-\left[{}_2F_1\left(2,4.5;3.75;\frac{v_-+v_+}{2v_+}\right)\right]}{512\sqrt{2}\pi^4\sqrt{-M_1}(v_-^2-v_+^2)^3v_+v_z/[\sqrt{v_-}\Gamma(1.25)]}\cos(2\varphi_R),
\end{aligned}\tag{B19}$$

where ${}_2F_1(a,b;c;t)$ is the Gauss hypergeometric function. Similarly, J_{zz} can be solved as

$$\begin{aligned}
J_{zz} &= \mathrm{Im}\int_{-\infty}^{0}\left\{\frac{K_{1/4}^2(-iR_\parallel\omega/v_-)-K_{5/4}^2(-iR_\parallel\omega/v_-)}{2M_1\pi^5R_\parallel^{1/2}v_+^{7/2}/\left[\lambda^2(1-i)\omega^{5/2}\Gamma^2\left(\frac{5}{4}\right)\right]}-\frac{\lambda^2(1+i)\omega^{3/2}K_{3/4}^2(-iR_\parallel\omega/v_-)\Gamma^2\left(\frac{7}{4}\right)}{9M_1\pi^5R_\parallel^{3/2}v_+^{5/2}}+\frac{\lambda^2(i2R_\parallel\omega-v_+)e^{i2R_\parallel\omega/v_+}}{2\pi^3R_\parallel^4v_+v_z^2}\right\}d\omega,\\
&= -\frac{\lambda^2}{15M_1\pi^3}\frac{1}{R_\parallel^4}+\frac{v_+\lambda^2}{2\pi^3v_z^2}\frac{1}{R_\parallel^5}.
\end{aligned}\tag{B20}$$

[1] M. Ezawa, Phys. Rev. Lett. **110**, 026603 (2013).
[2] M. S. Rudner, N. H. Lindner, E. Berg, and M. Levin, Phys. Rev. X **3**, 031005 (2013).
[3] P. Titum, N. H. Lindner, M. C. Rechtsman, and G. Refael, Phys. Rev. Lett. **114**, 056801 (2015).
[4] A. Farrell and T. Pereg-Barnea, Phys. Rev. Lett. **115**, 106403 (2015).
[5] C.-K. Chan, P. A. Lee, K. S. Burch, J. H. Han, and Y. Ran, Phys. Rev. Lett. **116**, 026805 (2016).
[6] M.-X. Deng, W. Y. Deng, D. X. Shao, R.-Q. Wang, R. Shen, L. Sheng, and D. Y. Xing, Phys. Rev. B **95**, 115102 (2017).
[7] Z. Yan and Z. Wang, Phys. Rev. Lett. **117**, 087402 (2016).
[8] H. Hübener, M. A. Sentef, U. D. Giovannini, A. F. Kemper, and A. Rubio, Nat. Commun. **8**, 13940 (2017).
[9] P.-H. Fu, H.-J. Duan, R.-Q. Wang, and H. Chen, Phys. Lett. A **381**, 3499 (2017).
[10] T. Nag, A. Menon, and B. Basu, Phys. Rev. B **102**, 014307 (2020).
[11] M. C. Rechtsman, J. M. Zeuner, Y. Plotnik, Y. Lumer, D. Podolsky, F. Dreisow, S. Nolte, M. Segev, and A. Szameit, Nature (London) **496**, 196 (2013).
[12] Y. H. Wang, H. Steinberg, P. Jarillo-Herrero, and N. Gedik, Science **342**, 453 (2013).
[13] X.-S. Li, C. Wang, M.-X. Deng, H.-J. Duan, P.-H. Fu, R.-Q. Wang, L. Sheng, and D. Y. Xing, Phys. Rev. Lett. **123**, 206601 (2019).
[14] M. Zare, F. Parhizgar, and R. Asgari, Phys. Rev. B **94**, 045443 (2016).
[15] G. C. Paul, S. K. F. Islam, and A. Saha, Phys. Rev. B **99**, 155418 (2019).
[16] H.-J. Duan, S.-H. Zheng, R.-Q. Wang, M.-X. Deng, and M. Yang, Phys. Rev. B **99**, 165111 (2019).
[17] G. C. Paul, S. K. F. Islam, P. Dutta, and A. Saha, Phys. Rev. B **103**, 115306 (2021).
[18] H.-J. Duan, S.-H. Zheng, Y.-Y. Yang, C.-Y. Zhu, M.-X. Deng, M. Yang, and R.-Q. Wang, Phys. Rev. B **102**, 165110 (2020).
[19] H.-J. Duan, Y.-J. Wu, Y.-Y. Yang, S.-H. Zheng, C.-Y. Zhu, M.-X. Deng, M. Yang, and R.-Q. Wang, New J. Phys. **24**, 033029 (2022).
[20] H.-R. Chang, J. Zhou, S.-X. Wang, W.-Y. Shan, and D. Xiao, Phys. Rev. B **92**, 241103(R) (2015).
[21] M. V. Hosseini and M. Askari, Phys. Rev. B **92**, 224435 (2015).
[22] H.-J. Duan, S.-H. Zheng, P.-H. Fu, R.-Q. Wang, J.-F. Liu, G.-H. Wang, and M. Yang, New J. Phys. **20**, 103008 (2018).
[23] M. M. Asmar and W.-K. Tse, New J. Phys. **23**, 123031 (2021).
[24] M. Yarmohammadi, M. Bukov, and M. H. Kolodrubetz, Phys. Rev. B **107**, 054439 (2023).
[25] M. Ke, M. M. Asmar, and W.-K. Tse, Phys. Rev. Res. **2**, 033228 (2020).
[26] M. Shiranzaei, J. Fransson, H. Cheraghchi, and F. Parhizgar, Phys. Rev. B **97**, 180402(R) (2018).
[27] Z. Wang, Y. Sun, X.-Q. Chen, C. Franchini, G. Xu, H. Weng, X. Dai, and Z. Fang, Phys. Rev. B **85**, 195320 (2012).
[28] Z. Wang, H. Weng, Q. Wu, X. Dai, and Z. Fang, Phys. Rev. B **88**, 125427 (2013).
[29] H.-J. Duan, S. Li, S.-H. Zheng, Z. Sun, M. Yang, and R.-Q. Wang, New J. Phys. **19**, 103010 (2017).
[30] K.-Y. Yang, Y.-M. Lu, and Y. Ran, Phys. Rev. B **84**, 075129 (2011).
[31] M. A. Ruderman and C. Kittel, Phys. Rev. **96**, 99 (1954).
[32] T. Kasuya, Prog. Theor. Phys. **16**, 45 (1956).
[33] K. Yosida, Phys. Rev. **106**, 893 (1957).

[34] D. C. Mattis, *The Theory of Magnetism Made Simple: An Introduction to Physical Concepts and to Some Useful Mathematical Methods* (World Scientific, Singapore, 2006).
[35] D. Mastrogiuseppe, N. Sandler, and S. E. Ulloa, Phys. Rev. B **93**, 094433 (2016).
[36] V. Kaladzhyan, A. A. Zyuzin, and P. Simon, Phys. Rev. B **99**, 165302 (2019).
[37] C. Laplane, E. Zambrini Cruzeiro, F. Fröwis, P. Goldner, and M. Afzelius, Phys. Rev. Lett. **117**, 037203 (2016).
[38] L. Zhou, J. Wiebe, S. Lounis, E. Vedmedenko, F. Meier, S. Blügel, P. H. Dederichs, and R. Wiesendanger, Nat. Phys. **6**, 187 (2010).
[39] F. Meier, L. Zhou, J. Wiebe, and R. Wiesendanger, Science **320**, 82 (2008).